PROCEEDINGS, 51st Workshop on Geothermal Reservoir Engineering
Stanford University, Stanford, California, February 9-11, 2026
SGP-TR-230

Combined Stimulation Mechanisms: Hydraulic Opening and Hydro-Shearing of an Existing Fracture

Ankit Gupta, Alexis Sáez, and Brice Lecampion

Geo-Energy Lab, Ecole Polytechnique de Lausanne, Station 18, CH-1015 Lausanne, Switzerland

brice.lecampion@epfl.ch

Keywords: Reservoir Stimulation, Hydraulic stimulation, hydraulic re-opening, hydro-shearing, fracture growth.

ABSTRACT

We investigate the growth of a hydro-shearing rupture along an existing fracture where the injection pressure is not controlled to remain below the fracture normal in-situ stress. As a result, hydraulic fracturing of the hydro-sheared fracture occurs (also named hydraulic jacking). We focus on the case of planar three-dimensional circular ruptures, which is geometrically simple yet practically relevant. We demonstrate that two fronts propagate along the existing fracture: a shearing front and an opening front. The latter follows the well-known zero-toughness (viscosity-dominated) solution for a penny-shaped hydraulic fracture, although pore fluid pressure diffuses ahead of the opening front. The shearing front lies ahead of the opening front with an amplification that depends on the stress criticality (in-situ shear stress over initial frictional strength), and the pore-pressure profile resulting from the leakage of fluid ahead of the opening front. Using scaling analysis and fully coupled hydro-mechanical simulations, we show that diffusion ahead of the opening front slowly becomes of order one at large times, with an intensity that mostly depends on the ratio between the characteristic over-pressure for radial fluid flow in the intact fracture and the in-situ normal effective stresses. The extent of the frictional shear rupture ahead of the opening front also depends on stress criticality, defined as the ratio between the initial shear stress and the initial frictional strength of the fracture.

1. INTRODUCTION

Hydraulic stimulation of pre-existing fractures is employed in geothermal development to increase reservoir permeability and achieve economical flow rates, though with mixed success (Jung 2013, McClure & Horne 2014). While the primary objective is to induce shear dilation of pre-existing discontinuities through fluid injection, field tests have demonstrated that substantial permeability increases are often observed when fracture opening is achieved - a phenomenon sometimes referred to as hydraulic jacking. Recognizing this, proppants have sometimes been injected with the scope of stimulation primarily aimed at reactivating existing fractures (Cornet, 2016, 2017).

In order to better design the re-activation of an existing natural fracture, one must understand the interplay between the evolution of a frictional rupture and the possible occurrence of fracture opening and subsequent propagation of an opening patch. By understanding the controlling parameters (in-situ conditions, natural fracture properties and injection operational parameters) for the evolution of the fluid-induced rupture along pre-existing fracture, it may become possible to maximize the increase of hydraulic transmissivity of the fracture.

Along similar lines to the plane-strain configuration (Lecampion et al 2023), we have investigated in 3D the shear-reactivation, then hydraulic opening of an existing planar fracture (see Fig. 1 for a schematic). For simplicity, we assume that fluid is injected at a constant volumetric rate Q in a fracture with an initial hydraulic aperture w_o. The injected fluid is assumed to have similar properties to the saturating formation fluid and to follow a Newtonian rheology with a fluid viscosity μ. Before the start of the injection, the fracture is in equilibrium under the action of the compressive in-situ stress field, and the in-situ pore-pressure p_o: both a normal σ_o and shear stress τ_o act on the fracture plane. Assuming a constant friction coefficient, we denote the ratio initial shear stress to initial fracture shear strength $S = \tau_o/f\sigma_o'$ as the stress criticality, with $\sigma_o' = \sigma_o - p_o$ denoting the initial effective normal stress.

In what follow, we briefly described the physical mechanism that must be accounted to understand how this existing fracture will react to fluid-injection – laying out the ingredients of the coupled hydro-mechanical problem without entering into the details of its mathematical formulation. We then discuss the different possible behaviors based on a scaling analysis of the problem. In particular, we present the dimensionless numbers controlling the problem. A set of numerical results is presented for the case of purely circular ruptures – highlighting the impact of stress criticality and of the amount of pore fluid pressure diffusion ahead of the opening zone. The relevance of our results for practical injection is then briefly discussed.

2. MODEL DESCRIPTION

We neglect any losses of fluid in the formation, such that all the injected fluid is assumed to enter into the existing fracture. Such an assumption is relevant for the case of a tight matrix (as seen with respect to the duration of the injection). The rock mass is assumed to be isotropic linear elastic, with uniform properties (Young's modulus E, and Poisson's ratio ν). All the non-linearities of the problem are associated with the hydromechanical constitutive behavior of the pre-existing fracture. We assume that it follows a simple elasto-plastic (rate-independent) non-associated Mohr-Coulomb behavior without any cohesion. Furthermore, for simplicity, we assume that once shear failure is activated, the plastic shear slip occurs without dilation (plastic slip at critical state).

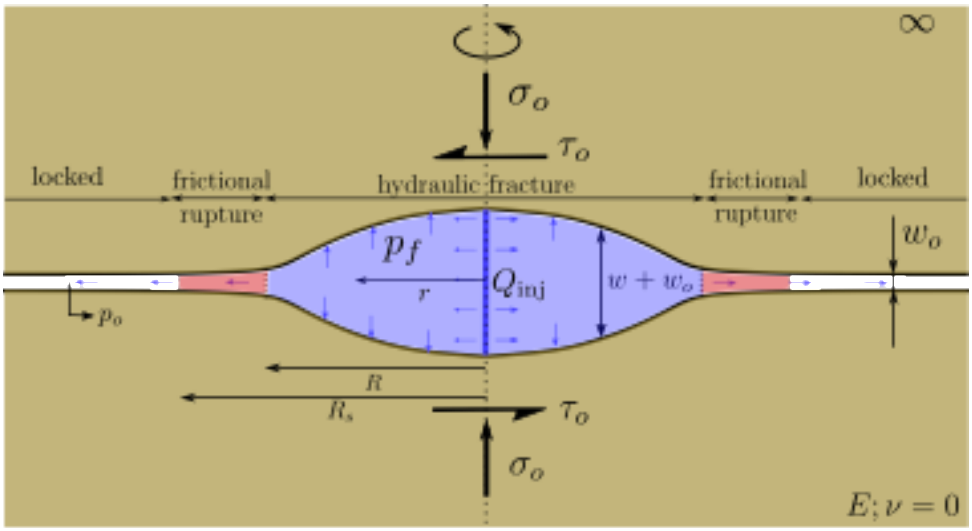

Figure 1 – Schematic of the combined shear activation and hydraulic re-opening of an existing fracture due to fluid injection – axisymmetric configuration. Both a normal and shear initial stress acts on the fracture prior to the start of the injection.

For a planar fracture, it is important to recognize that the mode of elastic deformation uncouples. In other words, shear slip does not modify the normal stress acting on the fault, while fracture opening does not modify the shear stress. In addition, in 3D, the geometry of the rupture remains strictly circular for the case of zero Poisson's ratio. However, the rupture area has been shown to be independent of the Poisson's ratio (Sáez et al 2022). We therefore present here only results for the case of circular rupture –, and the results can be directly translated in rupture area for any value of Poisson's ratio.

2.1 Initial characteristic fluid pressure & shear rupture activation

In the absence of mechanical coupling, fluid injection from a point source into the existing planar fracture with an initial hydraulic aperture w_o (and permeability kk) follows the well-known Theis solution. The fluid over-pressure is given by:

$$p(r,t) - p_o = \frac{\Delta p_c}{4\pi} E_1\left(\frac{r}{\sqrt{4\alpha t}}\right)$$

where $\alpha = k/(\mu S)$ is the initial fracture hydraulic diffusivity (with S its storage coefficient). The characteristic injection pressure Δp_c is given by

$$\Delta p_c = \frac{Q\,\mu}{k w_o} \tag{1}$$

Although the fluid overpressure is singular due to the point source, the pressure level is set by at the scale of a finite well-bore radius (see e.g. Saez & Lecampion 2024 – Appendix). As a result, if the characteristic pressure remains below the initial effective normal confining stress σ'_o, the fracture will not mechanically open. However, the pore-pressure increase due to fluid injection results in the activation and propagation of a frictional rupture (Garagash & Germanovitch 2012, Bhattacharya & Viesca 2019). Under the assumption of constant hydraulic properties (or assuming an infinite increase of permeability), the evolution of the frictional rupture is self-similar and is directly proportional to the evolution of the pore-pressure front $L = \sqrt{4\alpha t}$. Depending on the initial stress criticality S and amount of over-pressure (with respect to the initial fracture shear strength), the rupture front can lie ahead (critically stressed conditions) or behind (marginally pressurized conditions) the pore-pressure front.

If the characteristic injection over-pressure exceeds the initial effective normal confining stress σ'_o, the fracture will mechanically open. From the expression of the characteristic over-pressure (1), we directly see that large flow rates and/or small values of the initial hydraulic transmissivity of the fracture will result in large fluid over-pressure prone to fracture opening.

2.2 Zero-toughness hydraulic fracture in the absence of any initial shear stress

If the orientation of the fracture is such that no initial shear stress is present, If the orientation of the fracture is such that no initial shear stress is present, if the over-pressure is sufficient, the problem becomes similar to the propagation of a hydraulic fracture under the condition of negligible fracture energy (zero toughness case) – see Savitski & Detournay (2002) for the solution of a propagating radial hydraulic fracture under this condition. The evolution of the fracture radius, mechanical aperture and net loading respectively scales as (in this so-called viscosity-dominated regime):

$$R_m = \frac{E'^{1/9} Q^{1/3} t^{4/9}}{(12\mu)^{1/9}}, W_m = \frac{(12\mu)^{2/9} Q^{1/3} t^{1/9}}{E'^{2/9}}, P_m^{net} = \frac{E'^{2/3} (12\mu)^{1/3}}{t^{1/3}}$$

However, contrary to the classical hydraulic fracture model, fluid can flow ahead of the opening front as the pre-existing fracture has an initial hydraulic transmissibility kw_o. In fact, we can see from the hydraulic fracture scaling that the opening front propagates slightly slower $R \propto t^{4/9}$ than the characteristic pore pressure diffusion front $L = \sqrt{4\alpha t}$. This can be mathematically captured by the following dimensionless diffusivity

$$D = \frac{L^2}{R_m^2} = \bar{D} \times \left(\frac{t}{t_o}\right)^{1/9}$$

where $t_o = E'^2(12\mu)/\sigma_o'$ is the characteristic time for the occurrence of fracture opening (obtained by equalizing the characteristic hydraulic fracture net loading and the initial effective normal stress), and $\bar{D}$ is akin to a dimensionless diffusivity independent of time, defined as

$$\bar{D} = \left(\frac{\sigma'_o}{\Delta p_c}\right)^{2/3} \times (S\sigma'_o)^{-1}$$

It is first important to note that the increase of the dimensionless diffusivity with time is very slow (1/9 power) such that the intensity of the fluid flow ahead of the opening front is set by the value of $\bar{D}$. The latter is primarily influenced by the ratio $\Delta p_c/\sigma'_o$ (as the product of the initial storage coefficient and the initial effective normal stress $S\sigma'_o$ is always of order $O(10^{-3})$).

2.3 Non-zero initial shear stress: Evolution of the shear rupture front

As already mentioned, the mode of deformation uncouples for a planar fracture. As a result, the propagation of the opening front does not modify the shear stress acting on the fracture. However, it modifies the normal traction, and as fluid can flow ahead of the opening front the fluid pore-pressure can also rises (the Skempton effect can be shown to be of second order for stiff fracture – see Lecampion et al (2023)). As a consequence, the frictional strength of the fracture decreases. We therefore see that the evolution of the shear rupture front will depend on the amount of fluid diffusion ahead of the opening tip (captured by the value of $\bar{D}$) and the initial stress criticality ratio *S*.

It is important to note that in the absence of shear induced dilation (or when the latter is smaller than the characteristic width of the open patch), the propagation of the shear rupture does not influence the propagation of the opening front – thanks again to decoupling of opening and shear mode for a planar fracture.

3 NUMERICAL SOLVER

We briefly present the numerical solver used to simulate this problem – see Lecampion et al (2025) for details. Recognizing that all the non-linearities lie along pre-existing discontinuities, we use the traction hyper-singular boundary integral equation to solve the quasi-static balance of momentum of the rock using a boundary element method. More specifically, we discretize the pre-existing interfaces via piece-wise constant displacement discontinuity elements. We use a hierarchical representation of the otherwise densely populated resulting boundary element matrix. This ensures that both the memory and computational cost for a matrix vector product scale as O(n log n) – where n is the total number of degree of freedoms. The pre-existing interface behaves in a poro-elastoplastic manner, with softening of friction and a non-associated flow rule allowing to reproduce typical rock joint behavior towards critical state.

Fluid flow is discretized with a continuous Galerkin finite element method. Owing to the non-linearity associated with the evolution of hydraulic properties with fracture opening, and the strong hydromechanical coupling, we use a fully implicit time integration scheme. A classic elastic predictor–plastic corrector algorithm is used within a fully coupled Newton-Raphson algorithm at each time step. The solution of the fully-coupled Jacobian system is obtained using a nested iterative solver (BiCGStab) with a specifically designed block pre-conditioner. Its application requires the solution of the mechanical block, which is also obtained with an iterative solver thus leveraging the use of a hierarchical matrix for the boundary element method. This results in an accurate and robust solver.

4. NUMERICAL RESULTS AND DISCUSSION

To illustrate the previous discussion, we present a series of simulation for two different values of $\bar{D}$ (either greater or lower than unity) and different values of stress criticality. Figures 2 and 3 display the evolution of the shear rupture and opening fronts (as well as the pore-pressure front), and scaled fracture aperture, slip, and effective stresses profiles – both for a stress criticallity $S = 0.7$.

For the case of mininal pore-pressure diffusion ahead (small $\bar{D}$), depicted in Figure 2, we can see that the opening front closely follows the M-vertex HF solution (blue dashed line), and the diffusion front slightly outpaces the shear rupture front. for this value of *S*. For the various spatial profiles of the field variables along the fracture surface, Figure 2 (b) to (f), we have scaled each profile appropriately as discussed in Sec.~2, where each curve depicts a snapshot of the profile in time. As time evolves, the scaled opening and net pressure profiles, shown in panels (b) and (c) respectively, overlap with each other and match closely with the self-similar M-vertex solution. However, the fluid overpressure profile, shown in panel (d), shows mild deviation from self-similarity outside the HF. Consequently, the shear stress and slip profiles shown in panels (e) and (f) respectively also show deviation from self-similarity.

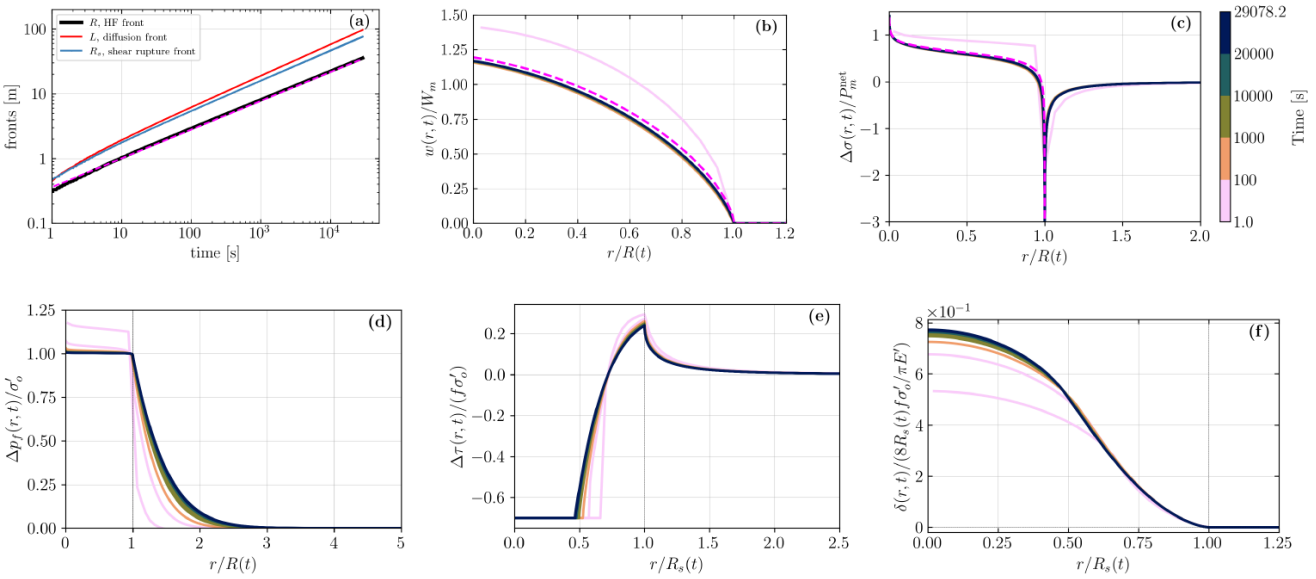

Figure 2 – Numerical results for a case with minimal diffusion ahead of the opening HF front $\overline{D} = 0.0424$. a) pore-pressure diffusion, shear rupture, and opening fronts evolution with time, scaled b) opening, c) net loading, d) fluid over-pressure, e) shear stress changes and f) slip profiles at different times (colour code on the top row right). The pink dashed line for the fracture opening and net loading profiles is the zero-toughness solution (Savitski & Detournay 2002).

Figure 3 corresponds to the case with significant diffusion ahead of the opening front (large $\overline{D}$). In panel (a), we again observe that the opening front closely follows the M-vertex HF solution (blue dashed line), and the diffusion front outpaces both the HF front and the shear rupture front. Panels (b) to (f) of Figure 3 show various scaled spatial profiles of the field variables along the fracture surface, where each curve again depicts a snapshot of profile in time. The scaled opening and net pressure profiles, shown in Figs. (b) and (c) respectively, show mild self similarity and clearly deviates from the M-vertex solution with time. This is because fluid flux coming out of opening tip scales with $\overline{D}$, enabling significant diffusion of fluid from the HF tip, which is also evident in the fluid overpressure profile, shown in panel (d). However, the fluid overpressure (panel (d)), the shear stress and slip profiles shown in panels (e) and (f) respectively are mildly self similar as time evolves.

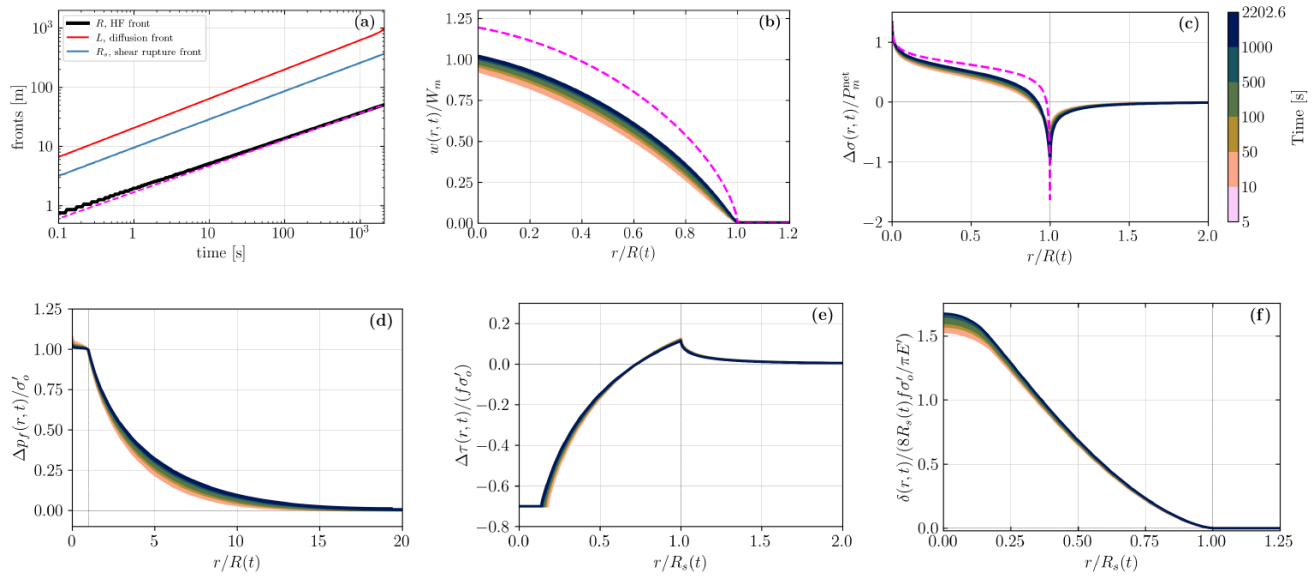

Figure 10 – Numerical results for a case with significant diffusion ahead of the opening HF front $\overline{D} = 4.24$. a) pore-pressure diffusion, shear rupture, and opening fronts evolution with time, scaled b) opening, c) net loading, d) fluid over-pressure, e) shear stress changes and f) slip profiles at different times (color code on the top row right). The pink dashed line for the fracture opening and net loading profiles is the zero-toughness solution (Savitski & Detournay 2002).

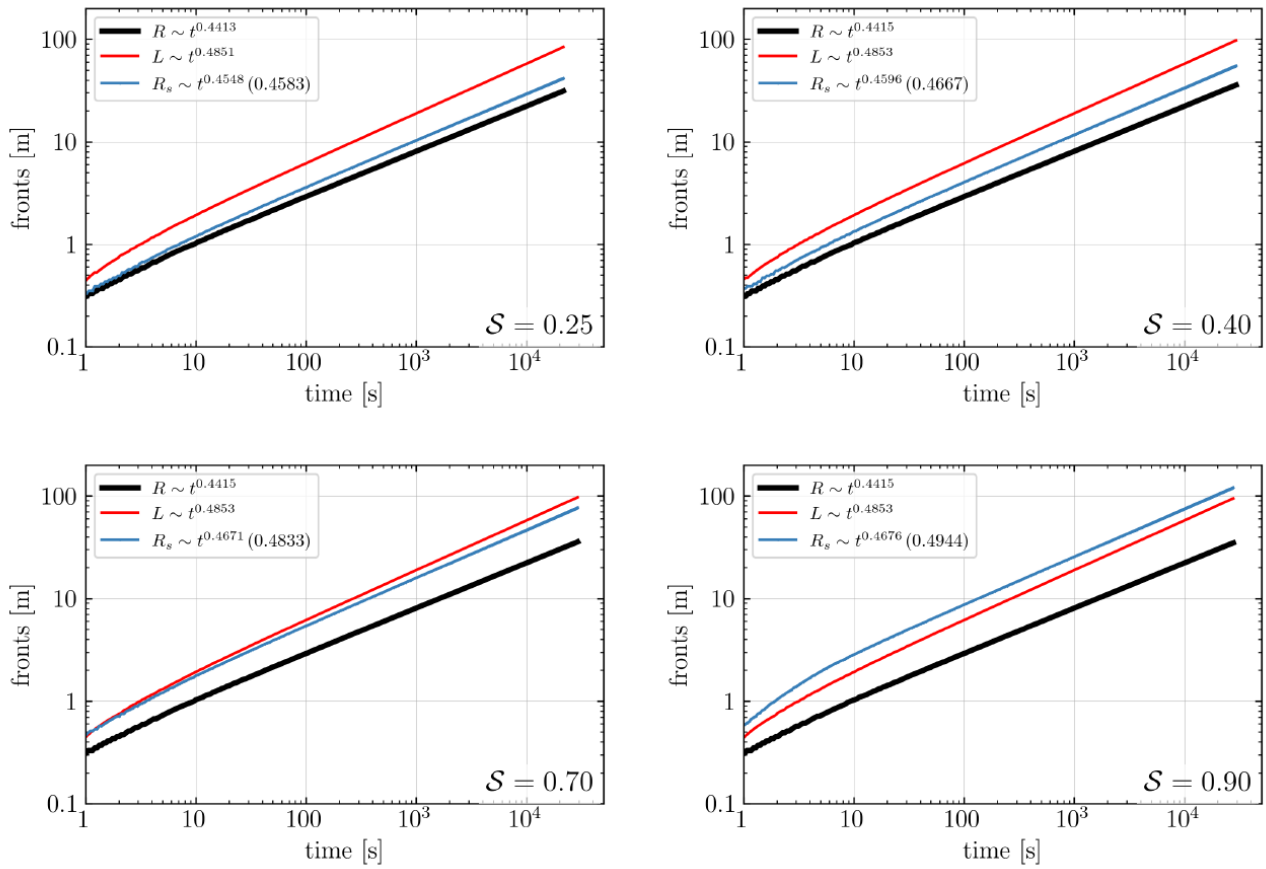

Figure 4 – Effect of the initial stress criticality $S = \tau_o/f\sigma'_o$ on the evolution of the pore-pressure diffusion front (blue), shear rupture front (red), and opening HF front (black) for a case with minimal diffusion ahead of the opening front ($\overline{D} = 0.0424$).

The impact of stress criticality $S = \tau_o/f\sigma'_o$ is reported on Figure 4 and 5 for minimal and significant diffusion ahead of the opening front respectively. We display the evolution of the rupture fronts and pore-pressure disturbance with time.

We observe (as expected) that the opening front is propagation is not affected by stress criticality (nor significantly by the value of $\overline{D}$). The position of the pore-pressure front (estimated as a 2% increase from the initial value of pore-pressure) of course is significantly ahead of the opening front for larger value of $\overline{D}$. It is, however, not dependent on *S*. The position of the shear rupture front is on the other hand function of both $\overline{D}$ and *S* . It increases for larger $\overline{D}$ and larger *S*.

5. CONCLUSIONS AND PERSPECTIVES

Fluid injection into an existing fracture will result first in shear activation. If the characteristic fluid overpressure (associated with Darcy's flow) exceeds the initial effective stress acting normal to the fracture plane, the fracture will open hydraulically. As a result, a hydraulic fracture front will propagate and further drive the shear rupture front. Because fluid can flow ahead of the opening front along the existing fracture, two regimes emerge – a small and a large diffusion regime. Although the opening front is not impacted by this diffusion ahead. The shear rupture front depends directly on the amount of diffusion ahead of the opening front (via the value of $\overline{D}$) as well as on stress criticality (via the value of *S*).

We hope that the clarification of the combined propagation of a shear rupture and opening front will allow to better rationalize some field observations. The dimensionless numbers presented here can be directly used to gain a first-order estimation of what to expect for a given set of operational parameters, in-situ conditions, and natural fracture properties.

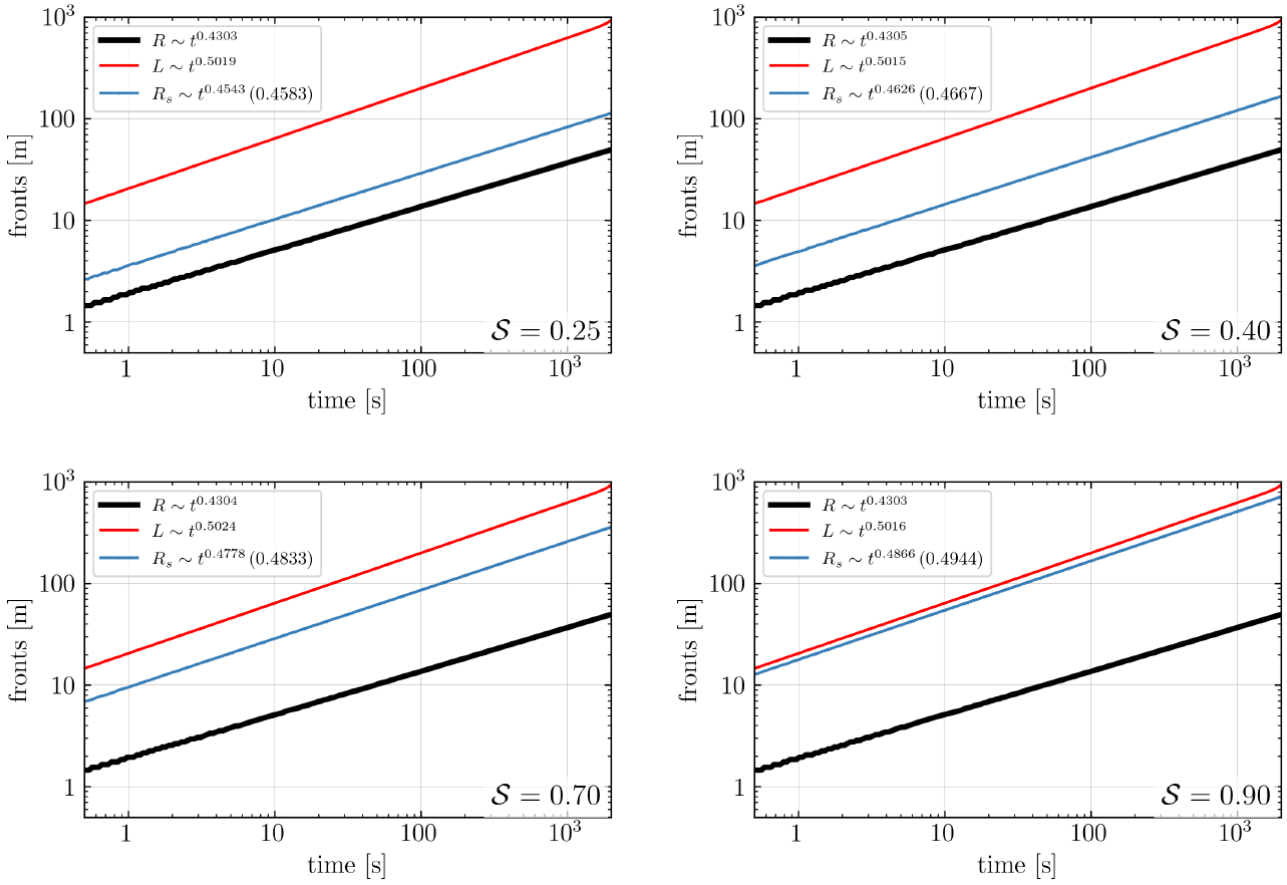

Figure 5 – Effect of the initial stress criticality $S = \tau_o/f\sigma'_o$ on the evolution of the pore-pressure diffusion front (blue), shear rupture front (red), and opening HF front (black) for a case with significant diffusion ahead of the opening front ($\overline{D} = 4.24$).

Acknowledgements

The results were obtained within the EMOD project (Engineering model for hydraulic stimulation). The EMOD project benefits from a grant (research contract no. SI/502081-01) and an exploration subsidy (contract no. MF-021-GEO-ERK) of the Swiss federal office of energy for the EGS geothermal project in Haute-Sorne, canton of Jura, which is gratefully acknowledged.

REFERENCES

1. M. W. McClure and R. N. Horne. An investigation of stimulation mechanisms in Enhanced Geothermal Systems. *Int. J. Rock Mech. Min. Sci.*, 72:242–260, 2014.
2. R. Jung. EGS - Goodbye or Back to the Future. In *ISRM International Conference for Effective and Sustainable Hydraulic Fracturing*. International Society for Rock Mechanics, 2013.
3. F. H. Cornet. Seismic and aseismic motions generated by fluid injections. *Geomechanics for Energy and the Environment*, 5:42–54, 2016.
4. F. H. Cornet. The engineering of safe hydraulic stimulations for egs development in hot crystalline rock masses. *Geomechanics for Energy and the Environment*, 26:100151, June 2021.
5. D. I. Garagash and L. N. Germanovich. Nucleation and arrest of dynamic slip on a pressurized fault. *Journal of Geophysical Research: Solid Earth (1978–2012)*, 117(B10), 2012.
6. P. Bhattacharya and R. C. Viesca. Fluid-induced aseismic fault slip outpaces pore-fluid migration. *Science*, 364(6439):464–468, 2019.
7. R. C. Viesca. Asymptotic solutions for self-similar fault slip induced by fluid injection at constant rate. *arXiv preprint arXiv:2401.13828*, 2024.
8. A. Sáez, B. Lecampion, P. Bhattacharya, and R. Viesca. Three-dimensional fluid-driven stable frictional ruptures. *J. Mech. Phys. Sol.*, 160:104754, 2022.
9. A. Sáez and B. Lecampion. Post-injection aseismic slip as a mechanism for the delayed triggering of seismicity. *Proceedings of the Royal Society A*, 479(2273):20220810, 2023.

10. B. Lecampion, A. Sáez, and A. Gupta. Shearing and opening of a pre-existing discontinuity in response to fluid injection. In *57th US Rock Mechanics/Geomechanics Symposium*, number ARMA 23-721, Atlanta, GA, USA, June 25–28 2023.
11. A. Sáez and B. Lecampion. Fluid-driven slow slip and earthquake nucleation on a slip-weakening circular fault. *J. Mech. Phys. Sol.*, page 105506, 2024.
12. E. M. Dunham. Fluid-driven aseismic fault slip with permeability enhancement and dilatancy. *Philo- sophical Transactions A*, 382(2276):20230255, 2024.
13. A. Savitski and E. Detournay. Propagation of a penny-shaped fluid-driven fracture in an impermeable rock: asymptotic solutions. *International Journal of Solids and Structures*, 39(26):6311–6337, dec 2002.
14. A. Sáez, F. Passelègue, and B. Lecampion. Maximum size and magnitude of injection-induced slow slip events. *Science Advances*, 11(19), May 2025.
15. P. Wriggers. *Computational contact mechanics*. Springer Science & Business Media, 2006.
16. B. Lecampion, F. Fayard, A. Gupta, C. Peruzzo, A. Sáez, N. Richart, D. Nikolskiy, and F. Ciardo. BigWham: a C++ library for vectorial Boundary InteGral equations With HierArchical Matrices, Feb. 2025.
17. B. Lecampion, A. Gupta, A. Sáez, R. Fakhretdinova, A. Sarma, and S. Brisson. A robust numerical solver for the simulation of fluid-driven ruptures on pre-existing discontinuities in fractured rocks. In *Proceedings of the Third International Conference on Energy Geotechnics*, Paris, France, June 17-20, 2025.